Journal of Constructional Steel Research 188 (2022) 107038

Contents lists available at ScienceDirect

Journal of Constructional Steel Research

journal homepage: www.elsevier.com/locate/jcsr

# Investigating the redundancy of steel truss bridges composed of modular joints

Mirela D. Tumbeva [a], Ashley P. Thrall [a,*], Theodore P. Zoli [b]

[a] Kinetic Structures Laboratory, Department of Civil and Environmental Engineering and Earth Sciences, University of Notre Dame, Notre Dame IN 46556, USA
[b] HNTB Corporation, 57th Floor, Empire State Building, 350 5th Ave, New York, NY 10118, USA

ARTICLE INFO

*Keywords:*
Modular construction
Member loss
Redundancy
Resilience

ABSTRACT

The objective of this paper is to present a numerical investigation of the redundancy of steel truss bridges composed of novel modular joints when subjected to the sudden loss of diagonal members. The modular joint - a prefabricated steel nodal connector composed of flat web plate welded to flat and curved cold bent flange plates - represents a new approach to the construction of steel truss bridges in which the connector is a module that joins member that are standard rolled wide flange sections. A unique feature of this approach is that a moment-resisting connection is achieved in a truss topology by joining webs and flanges independently through bolted splice connections. This, in combination with orienting members in strong axis bending, provides the potential for the system to tolerate the loss of a diagonal member through load redistribution in flexure. The response of a 119-m (390-ft) simply supported vehicular bridge following the abrupt loss of a diagonal is numerically investigated considering three behaviors: (1) instantaneous dynamic behavior, focusing on the effect of the high-velocity stress wave, with its associated high strain rates and impact on fracture toughness particularly in the cold bent and welded portion of the modular joint, (2) short-term dynamic behavior of the structure, and (3) static behavior of the faulted structure. Results show that the modular joint is able to redistribute load after sudden member loss, demonstrating the redundancy of this new approach to modular construction.

## 1. Introduction

The modular joint (Fig. 1, [1]) is a new approach to the rapid fabrication and erection of steel truss bridges, where the module is the joint and members are standard rolled wide flange sections. The modular joint is a prefabricated built-up section composed of a flat web plate welded to flat and curved flange plates as shown in Fig. 1A. The curved flanges are cold bent to a prescribed radius to achieve the desired angle between members. A straight starter segment connects to other modular joints or to wide flange members. In this approach, a truss-like topology is formed using the modular joint repeatedly throughout the entire structure. For example, short span bridges are achieved by connecting modular joints to one another (Fig. 1B), whereas bridges with longer spans are developed by connecting modular joints to wide flange members (Fig. 1C).

For both short- and long-span bridges, bolted splice plate connections (in double shear) are used to independently connect the webs and flanges. This, combined with the strong axis orientation of the wide flange members, enables flexure to be transmitted in a truss-like topology and provides the potential for the structure to tolerate the loss of a diagonal member. This potential to tolerate the loss of a member makes the system load-path redundant [2] and is a unique feature of truss bridges comprised of modular joints compared to conventional trusses which are not able to tolerate member loss. Thus, the modular joint system aims to achieve enhanced resiliency through load-path redundant design.

The modular joint developed in Tumbeva et al. [1] is inspired by the "gussetless" Memorial Bridge connecting Portsmouth, NH and Kittery, ME. Like the Memorial Bridge, bridges composed of modular joints achieve the efficiency of a truss while eliminating the gusset plates which are prone to durability and maintenance problems, are difficult to fabricate and inspect, and are inefficient as fasteners are used in single shear [3]. Different from the Memorial Bridge, the modular joint system proposed in Tumbeva et al. [1] and investigated in this paper is modular, meaning identical joints can be used throughout the structure and among many different structures. While the Memorial Bridge was a one-of-a-kind design with sections fabricated in large pieces to minimize field splices, the modular joint approach focuses on small modules

* Corresponding author.
*E-mail addresses:* mtumbeva@nd.edu (M.D. Tumbeva), athrall@nd.edu (A.P. Thrall), tzoli@hntb.com (T.P. Zoli).

https://doi.org/10.1016/j.jcsr.2021.107038
Received 30 July 2021; Received in revised form 6 October 2021; Accepted 2 November 2021
Available online 22 November 2021

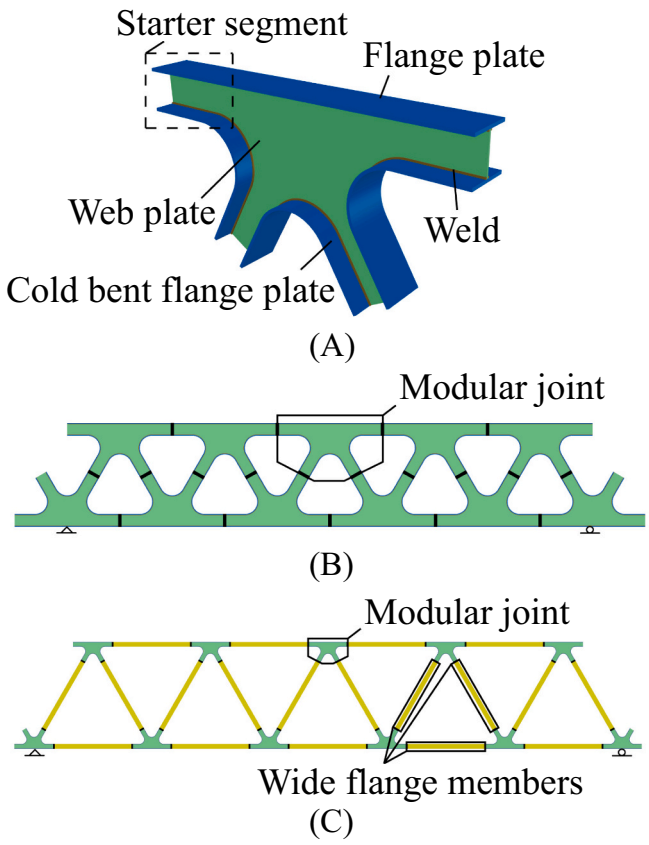


**Fig. 1.** Steel bridges composed of modular joints: (A) Modular joint, (B) Short-span constant-depth bridge, and (C) Long-span constant-depth bridge (reprinted from [1], © ASCE)

connecting standard wide flange sections, allowing for the accelerated fabrication and erection of the bridge. The modular joint system can be stacked in ISO (International Standard Organization) shipping containers for ease of transportation to a wide range of sites. These advantages make the modular joint system particularly useful for accelerated bridge construction as well as for disaster relief and military operations.

The modular joint utilizes the same fabrication techniques as the knuckle of the Memorial Bridge which has been experimentally tested and validated. For example, vibrations induced by span lifting and traffic loads were measured using camera-based field monitoring [4]. Shahsavari et al. [5] investigated live load behavior of the bridge by field monitoring using accelerometers, uniaxial strain gauges, strain rosettes, and tiltmeters. Bell and Medina [6] experimentally tested a scaled model of the knuckle under cycling load to evaluate the fatigue performance. Results showed that an infinite fatigue life is expected. A fatigue evaluation of the knuckle was also conducted by Mashayekhi and Santini-Bell [7] through both field measured data and numerical modeling.

In Tumbeva et al. [1], the authors have previously (1) developed the geometry of the modular joint, (2) developed methodologies for achieving constant- and variable-depth bridges, and (3) performed sizing optimization of the modular joint and wide flange sections for lowest weight while meeting geometric and structural constraints. In Tumbeva et al. [1], research focused on the static behavior of steel bridges comprised of modular joints. The novelty of the current paper is in understanding the dynamic behavior of the system after sudden member loss using explicit dynamic analyses, as well as an investigation of the behavior of the faulted structure through nonlinear static analysis. Specifically, this research focuses on the effect of the high-velocity stress wave instantaneously released after a member is damaged on the fracture toughness of the joint components as well as the ability of the modular joint to redistribute load.

A key factor to bridge durability and robustness is ensuring sufficient fracture toughness of the bridge steel components. The American Association of State Highway and Transportation Officials *LRFD Bridge Design Specifications* (AASHTO hereafter) includes minimum Charpy V-notch (CVN) test requirements to specify fracture toughness [8]. These requirements were developed in the beginning of the 1970's, partially prompted by the Silver Bridge near Point Pleasant, West Virginia collapse in 1967 with the goal to prevent unstable crack propagation and brittle failure. It is, however, typical for bridge steels to experience crack initiation and propagation at moderate stress levels throughout the bridge lifespan. Hence, increasing the fracture toughness might have a minor effect on the steel during normal service conditions [9]. Yet, bridges built prior to the introduction of fracture toughness requirements, and thus used low toughness steel, have exhibited unstable crack growth resulting in bridge closure. With the improvements in the bridge design code to include fracture toughness requirements and include fatigue design provisions, brittle fracture and fatigue cracking in bridges built after 1985 is extremely rare [10].

When introducing a new concept for steel bridges, as is the case of the modular joint system, it is important to establish component behavior and fracture toughness demand. Fracture toughness is primarily dependent on three key factors: (1) plate thickness, (2) service temperature and (3) loading rate, with a reduction in toughness associated with thicker plate, lower temperature, and higher loading rate [9]. The event of a sudden loss of a member is associated with a stress wave propagating at a very high rate [e.g, 5189 m/s (17024 ft/s) for steel]. This type of dynamic load significantly impacts the fracture toughness of the steel and thus, particular attention should be given to the modular joint's cold-worked flanges and the flange-to-web welds which are subjected to higher localized stress to avoid crack formation and crack propagation. This is specifically important because the cold bending of the flange plates and welding of the components already reduce the fracture toughness of the material.

To evaluate modular joint performance during a sudden member loss event, a key consideration is to establish component demands and strain rates consistent with this type of member loss event. In the development of fracture toughness requirements for bridge steels, Barsom [9] demonstrated the relationship between temperature and strain rate, with a reduction in fracture toughness associated with lower temperatures and higher strain rates, in contrast to yield and ultimate strengths. To evaluate the potential for fracture in the modular joint, it is necessary to establish strain rates associated with abrupt member loss, which are clearly different from the intermediate loading rates typical of live load passage over a bridge (loading time $> 1$ s corresponding to a strain rate of less than $10^{-3}$/s).

Importantly in the modular joint system, the members are rolled wide flange sections (i.e., no welds) and thus a reduction in fracture toughness during a high strain rate event is of less concern. Therefore, the major focus of this paper is the behavior of the modular joint immediately following the fracture of a diagonal member.

It is also important to understand the global behavior of the system and evaluate its ability to continue to carry load as well as maintain functionality. A key aspect in the modular joint system is the ability to redistribute load through flexure as a result of the moment-resisting connection between components and strong axis orientation of members, allowing bridges composed of modular joints to be classified as redundant.

This paper presents the redundancy analysis of the system and proposes a numerical approach for redundancy evaluation of steel bridges, that specifically considers the impact of the high-velocity stress wave. This numerical approach could also be used for other forms (i.e., variable-depth), other span arrangements, or for bridges that are not composed of modular joints.

## 2. Background

Redundancy of bridge structures can be classified into three categories: (1) internal member redundancy associated with built-up sections where individual plates are connected to form a section, (2) structural redundancy, associated with the static indeterminacy (e.g. continuous spans), and (3) load-path redundancy, associated with the ability of the structure to redistribute the load to members adjacent to a failed member and the capacity of these members to carry that load [2]. The focus of this paper is to investigate the load-path redundancy of constant-depth simply supported bridges composed of modular joints (Fig. 1C). Load-path redundancy can be evaluated through: (1) linear elastic static analysis, (2) nonlinear static analysis, (3) linear elastic dynamic analysis, and (4) nonlinear inelastic dynamic analysis [11]. This paper uses nonlinear inelastic dynamic analysis, which will be discussed in detail later in subsequent sections.

Conventional bridge design does not specifically account for redundancy but rather leaves this to the engineers' judgment and experience [2]. The American bridge design code [8] incorporates load factors in the strength limit states depending on the level of redundancy of the structure. If the bridge is classified as non-redundant, the load is increased, and if the system has a very high level of redundancy, the load is decreased [8].

A quantitative approach for evaluating the redundancy of prestressed concrete and steel bridge superstructures was developed by the National Cooperative Highway Research Program (NCHRP) Report 406 Redundancy in Highway Bridge Superstructures [12]. A set of system factors were introduced which can be applied to the nominal resistance of each member. The system factors were developed by considering the level of redundancy of the entire system as opposed to only considering individual members. To ensure a minimum level of system redundancy, four limit states were defined: (1) member failure limit state for ensuring sufficient member capacity, (2) ultimate limit state for ensuring capacity of the entire system under increased truck loading, (3) functionality limit state for ensuring traffic safety defined as the peak displacement due to live load, and (4) damaged condition limit state for ensuring safety of the structure in the case of a member loss. These system factors were later calibrated for the design and safety assessment of highway bridges subjected to lateral and vertical vehicular loads by the NCHRP Report 776 Bridge System Safety and Redundancy [13].

The most recent development in evaluating steel bridge redundancy is NCHRP Report 883 Fracture-Critical System Analysis for Steel Bridges [14], culminating in Guide Specifications for Analysis and Identification of Fracture Critical Members and System Redundant Members [15]. NCHRP Report 883 developed a methodology to determine if a member is fracture critical (FCM) or instead can be considered as a system-redundant member (SRM). It also proposed guidelines for bridge design and evaluation. To determine if a member is SRM, a numerical modeling approach was proposed and two load combinations were developed: (1) Redundancy I, relating to instantaneous member loss, and (2) Redundancy II, for evaluating the static behavior of the faulted structure. In the Redundancy I load combination, a dynamic amplification factor of 1.4 is introduced to account for the inertia effects, such that the behavior of the system can be investigated through static analysis. In this paper, the Redundancy I load combination is used in an explicit dynamic analysis to evaluate both the instantaneous and short-term dynamic behavior of the modular joint system. Thus, the dynamic amplification factor is not included. The Redundancy II load combination is used when the long-term behavior of the faulted structure is evaluated.

Typically, truss bridges are non-redundant and failure of a member can result in the collapse of the entire structure. Extensive research has been conducted on investigating the redundancy of truss-type structures. The Fatigue Evaluation and Redundancy Analysis report on the I-35W Bridge over the Mississippi River prepared by URS Corporation [16] included identifying the FCMs as well as evaluating the probability of collapse if member failure occurs. To consider the dynamic behavior due to the sudden member loss, the damaged structure was idealized as a single-degree-of-freedom system and the loss of the member was represented by a pulse force. The report assumed a 5% damping resulting in a dynamic impact factor (i.e., an amplification factor that accounts for inertial effects without performing a dynamic analysis) of 1.854. Additionally, recommendations for improving the redundancy of the bridge were proposed.

Cha et al. [17] experimentally and numerically evaluated the behavior of a simple span truss bridge when the lower chord is fractured. The studied bridge is composed of built-up sections which also provide internal member redundancy. The bridge was initially loaded to two-thirds of the design live load. The lower chord member at midspan was then partially damaged, and later the same member was completely fractured. The free vibration of the structure was recorded. Results from the experimental tests and finite element (FE) analysis (assuming nonlinear geometry and nonlinear material properties) showed that the force in the fractured lower chord was distributed to the adjacent diagonal members as well as to the lower chord in the opposite truss plane thus, allowing the bridge to continue to carry load even when the lower chord member was completely severed.

Yan et al. [18] investigated the resistance of planar trusses to collapse in the case of a damaged member through numerical and analytical approaches. Nonlinear dynamic models, including material nonlinearity, were used to analyze the truss when a member is suddenly removed. Two resisting mechanisms were established: catenary action if an upper chord member is damaged and arch action if a lower chord member is damaged. If a diagonal member is fractured, the response was found to be a combination of both collapse-resistant mechanisms.

Khuyen and Eiji [19] proposed a linear redundancy approach that incorporates the plastic strength of the members to identify FCM in steel truss bridges. The approach allows for a more accurate representation of the progressive collapse of the structure in the case of a sudden member loss in comparison with linear static analyses. The dynamic effects are incorporated through a dynamic impact factor which amplified the forces acting in the failed member.

Goto et al. [20] numerically estimated the dynamic impact factor through dynamic analyses for two Warren trusses when a tension member suddenly fails. Linear geometry and elastic material properties were assumed. A simplified method to approximate the dynamic impact factor using the root mean square mode combination method, which did not require a full dynamic analysis, was also proposed.

Liu et al. [21] numerically investigated the alternative load-path of the Grand River Bridge in Cayuga, Canada by removing an individual member from the structure before any load is applied. Material and geometric nonlinearities were incorporated in the models. However, dynamic effects were neglected. Fragility curves were developed to identify the bridge safety by accounting for uncertainties associated with load-path redundancy analysis.

Thai and Kim [22] proposed a numerical approach that included material and geometric nonlinearities to investigate the dynamic behavior of steel trusses under earthquake loading. Results indicated that the developed approach is capable of capturing different failure modes, including buckling, yielding, inelastic post-buckling.

Miyachi et al. [23] numerically investigated the effect of the span lengths and live load location on the progressive collapse of three-span continuous steel truss bridges by incrementally applying the live load until the structure collapses. Evaluation of ductility, estimated as the ultimate load over the yield load, was also performed. The analyses were carried out for two bridges with total span length of 230 m (755 ft). Nonlinear geometry and material properties were assumed. Results showed that both bridges experienced buckling failure, however, the bridge with a longer center span was more ductile. When the live load was at the side spans, longer side spans resulted in a higher ultimate strength, whereas when the live load was near the inner supports, a longer center span resulted in a higher ultimate strength. The different

combinations of span lengths did not affect the ultimate strength when the live load was positioned at the center span.

## 3. Objectives and scope

The objective of this research is to numerically investigate the behavior of steel truss bridges composed of modular joints when subjected to the sudden loss of a diagonal member. Specifically, the behavior of a 119-m (390-ft) simply supported, two-lane vehicular bridge is investigated through high-fidelity, three-dimensional (3D) FE analyses. This study numerically investigates three behaviors: (1) instantaneous behavior immediately following member loss, focusing on the effect of the high-velocity stress wave, (2) short-term dynamic behavior of the structure following member loss, and (3) static behavior of the faulted structure. The focus is on the local behavior of the modular joint (especially the location of the weld between the bent flanges and the web), as well as the global behavior of the system. Ultimately, the paper demonstrates the ability of the modular joint to redistribute load after sudden loss of a diagonal member. A simple case study of a wide flange beam is also presented to evaluate modeling methods and assumptions.

## 4. General features of bridge geometry and numerical models

This paper presents a numerical investigation of the redundancy of a 119-m (390-ft) simply supported, two-lane [9.91-m (32.5-ft) wide] vehicular bridge composed of modular joints, developed in Tumbeva et al. [1]. The modular joint is a built-up section of: 44.5 mm (1.75 in.) thick webs, 50.8 mm (2 in.) thick bent left and right flanges, 12.7 mm (0.5 in.) thick bent middle flange, and 34.9 mm (1.375 in.) thick flat bottom flange (Fig. 1A). The bridge consists of W14×233 lower chord members, W14×193 upper chord members, W14×193 portal diagonal members, and W14×109 diagonal members. W14×132 lateral bracing and W14×132 portal braces are incorporated for stability of the upper chord. These are joined to the modular joints via 25.4-mm (1-in.) thick flat plates and 38.1-mm (1.5-in.) thick stiffeners. W14×159 floor beams are positioned at every 3.05 m (10 ft) along the span length and are connected to the to the lower chord beams or lower chord modular joints through 38.1-mm (1.5-in.) thick stiffeners (Fig. 2).

The section sizes of the lower chord, upper chord, and diagonal members, as well as the thickness of the flange and web plates of the modular joint, were determined through sizing optimization [1]. The self-weight of the system was minimized while meeting structural (related to fatigue of the modular joint, global system stability, ultimate behavior, and failure mechanism) and geometric (related to transpotability and limiting strains from cold bending in the flange plates) constraints. The structural constraints were evaluated through a high-fidelity parametric 3D FE static analysis in ABAQUS [24].

The behavior of this system when a diagonal member is suddenly lost is evaluated using a high-fidelity 3D FE model in ABAQUS [24]. This model is based on the 3D FE model developed in Tumbeva et al. [1]. However in Tumbeva et al. [1], research focused on the static behavior of steel bridges comprised of modular joint, whereas the current paper focuses on understanding the dynamic behavior of the system after sudden member loss using explicit dynamic analyses, as well as an investigation of the behavior of the faulted structure through nonlinear static analysis. Thus, while the geometry of the FE model is similar, the analysis is very different and is a unique aspect of the dynamic performance of the modular joint given abrupt member loss.

Because a sudden loss of a tension member is associated with energy release in the form of a stress wave propagating through the member at a very high rate, the response of the system is dynamic and therefore, in this paper an explicit dynamic analysis is performed. This analysis is also required to determine the strain rates that are developed during member loss event and evaluate modular joint performance.The static analysis evaluates the long-term behavior of the faulted structure, simulating the post-fracture event response and reserve strength.

The additional assumptions (i.e., large deformation, material model,

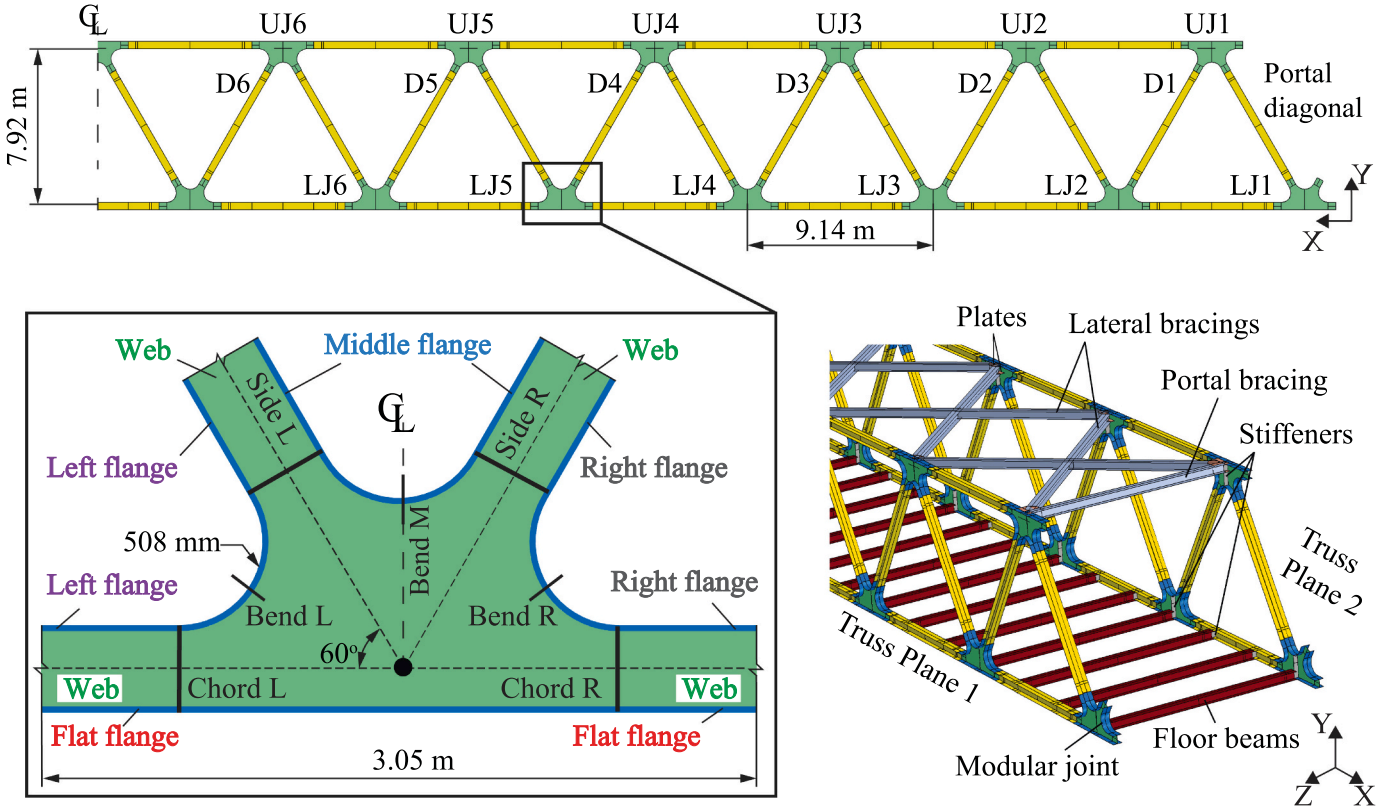


**Fig. 2.** Bridge geometry and 3D FE model.

mesh size) to the 3D FE model are made to reflect the complexity of these analyses and particularly to be able to capture the high-velocity stress wave released instantaneously after the member is fractured.

All bridge components are modeled with S3R or S4R (3- or 4-node) reduced integration general-purpose shell elements, both with six degrees of freedom at each node - thee translational and three rotational degrees of freedom. These general-purpose shell elements are capable of achieving full interaction between bending moments, shear, and axial forces. These elements, in addition to being computationally efficient, are suitable for modeling curved and flat shells that can exhibit nonlinear material response as well as undergo large deformation, and therefore, are the preferable choice for the current study. However, a comparison between different elements types (e.g., brick, shell, and beam elements) is also conducted and presented later in this paper.

A mesh refinement study, discussed in the following section, was performed to determine an appropriate mesh size for the current study. It is important to use the correct mesh size as it affects the accuracy of the solution and more specifically the response of the system to the high-velocity stress wave.

Grade 50W structural steel is used for all components in the model, assuming a stress-strain relationship with linear strain hardening [15] with the following properties: specified minimum yield strength of 345 MPa (50 ksi), ultimate strength of 483 MPa (70 ksi), peak strain at failure of 0.05, modulus of elasticity of 200 GPa (29,000 ksi), density of 7850 kg/m$^3$ (490 lbs/ft$^3$), and Poisson's ratio of 0.3. Note that the FE model developed in Tumbeva et al. [1] used an elastic-perfectly plastic material model with no strain hardening. However in the event of a sudden member loss, the structure is expected to redistribute load through ductile behavior and develop a collapse-resistant mechanism. Thus, nonlinear material properties including strain hardening would be able to represent this type of response.

Because the system undergoes sudden changes in geometry, due to member being fractured, causing the development of large deflections, the 3D FE model in this paper also incorporates nonlinear geometry. The model in Tumbeva et al. [1] assumed linear geometry as the response was expected in the liner elastic range.

Nonlinearity of any type typically requires iterations until convergence is satisfied and the system is in equilibrium. In this paper, the software ABAQUS [24] is used hence, analysis convergence criteria are automatically defined by the software. This is primarily valid when the global static behavior of the system is investigated. For nonlinear static problems, ABAQUS [24] calculates the force residual at each iteration and compares with a tolerance value that is set to 0.5 %. Additionally, a displacement correction is calculated and compared to the total increment displacement. Convergence is satisfied, meaning the system is considered in equilibrium, if the force residual is less than the tolerance value as well as the displacement correction is less than 1%.

In comparison, the explicit dynamic analysis solves for the displacement and velocities at the current time increment using the already known displacement and velocities from the previous time increment and therefore, iterations and convergence tolerances are not required. The accuracy of the solution to the dynamic problem depends on the stability limit which in this paper is automatically utilized by ABAQUS [24]. Specific details on the dynamic analysis and the stability limit are provided in the following section.

The splice connections between joints and members are not explicitly modeled. Instead, surface-to-surface or node-to-surface constraints tie all degrees of freedom of the connected nodes. Specifically, all nodes along the edges of the flanges of the members are tied to the nodes along the edges of the flanges of the modular joints. Similarly, the nodes along the web edge of the members are tied to the nodes along the web edge of the modular joints. The constraint ties all degrees of freedom at the nodes throughout the duration of the analysis. The same approach is used for connecting the plates to the upper chord modular joints and bracing, as well as for connecting the stiffeners to the lower chord members and modular joints.

The bridge deck is not physically included in the model. Instead, the weight of the deck is applied as a pressure at the top flange of the floor beam. The boundary conditions are: at one end of Truss Plane 1, translation is restrained; at the same end of Truss Plane 2, translation is restrained in longitudinal and vertical directions; at the other end of Truss Plane 1, translation is restrained in transverse and vertical directions; at the same end of Truss Plane 2, translation is restrained in vertical direction. The boundary conditions are applied at the node that is at the center of the flat flange of the each of the end lower chord joints.

## 5. Instantaneous dynamic behavior

This section investigates the instantaneous loss of a diagonal member, focusing on the effect of the high-velocity stress wave propagating through the member and modular joint immediately after it is severed. The stress wave travels with a very high speed, resulting in strain rates significantly above the intermediate strain rate of $10^{-3}$/s typical of live load passage over a bridge. These high strain rates are associated with lower fracture toughness of the steel, which combined with the reduced fracture toughness due to cold bending and welding increase the probability of crack formation and crack propagation in the joint components. Thus, it is particularly important to establish strain rates caused by abrupt member loss.

As described earlier, there are different procedures to simulate member loss. Zoli and Woodward [25] provided guidelines for modeling abrupt cable loss applicable for cable stayed, suspension, and arch bridges that can also be extended to truss bridges. An explicit dynamic analysis is proposed, in which the fractured member is removed from the model geometry. The load in the member (found through an analysis of the structure in the undamaged state) is applied at the two nodes connecting the member, but in opposite direction through a quasi-static time step. This compensates for the member removal and allows the structure to return to its initial (undamaged) stress state. Once the steady-state is reached, the load is abruptly decreased to zero, simulating the sudden member loss. In this paper, the method is referred to as *QSD*.

The time-dependent forcing function used in the *QSD* method is schematically shown in Fig. 3A, in which $t_r$, $t_h$, and $t_d$ refer to the load rise time, load hold time, and load release time respectively. The quasi-static portion of the function is the summation of the two times, $t_r$ and $t_h$. When the quasi-static time ends, the load release begins, and after time $t_d$, it ends at $t = 0$. After that, the structure is allowed to oscillate freely.

A limitation in using the *QSD* method is that during the quasi-static step the load must be applied very slowly, as the rise time, $t_r$, must be approximately four times the natural period of the structure [26], such that inertia effects are minimized and the kinetic energy is close to zero thus, achieving a static solution. For the simply supported bridge investigated in this paper, this type of analysis becomes a numerically challenging problem, as the natural period of the undamaged structure

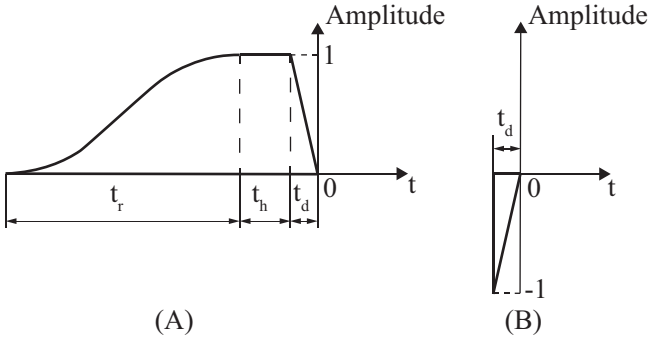


**Fig. 3.** Forcing function for dynamic analysis: (A) *QSD* method and (B) *SD* method.

is 3.11 s, requiring a very long load rise time, $t_r$, of approximately 12 s. To ensure that steady-state is reached, the load hold time, $t_h$ is approximately twice this period, further lengthening the quasi-static step.

The explicit dynamic analysis method uses the central-difference operator to solve the equation of motion, which is conditionally stable if the time increment, $\triangle t$, is sufficiently small (i.e. in the order of $10^{-3}$ ms), thus requiring a large number of time increments to reach a solution. This typically is not a problem, as the explicit method is primarily used to solve short time, high speed events. Furthermore, the method is highly efficient as the displacement and velocities at the current time increment are computed using the already known displacement and velocities from the previous time increment and therefore, the global mass and stiffness matrices do not need to be inverted. However, as described earlier, the bridge investigated in this paper requires a long quasi-static time step that would result in a very large number of increments and might not be capable of reaching the static solution.

To avoid the above-mentioned numerical challenges, in this paper behavior after sudden member loss is investigated through the following method: (1) a static analysis on the undamaged structure is performed to determine the initial (undamaged) stress state of the system, (2) this initial stress state is imported into another model in which the fractured member is separated into two parts by removing a number of elements from the member geometry along the cross-section, (3) a force with equal magnitude and opposite direction to the force acting on those elements prior to damage is applied at the failure surfaces, and (4) an explicit dynamic analysis is carried out in which the force is instantaneously decreased to zero in time, $t_d$ (Fig. 3B), and the structure is let to vibrate freely. In this method, the initial (undamaged) stress state serves a starting point for the dynamic analysis, meaning that the new displacements and forces are calculated on the already deformed configuration. In this paper, this method is referred to as *SD*. Note that, in both *QSD* and *SD*, the free vibration phase starts at $t = 0$, which is at the end of the load release time, $t_d$. A direct comparison of the *QSD* and *SD* methods is performed through a case study of a single beam discussed later in this section.

The results from both *QSD* and *SD* analysis depends on the time increment used in the explicit central-difference method to solve the equation of motion. The accuracy of the solution is controlled by the largest time increment, referred to as the stability limit, $\triangle t_{st}$, that is a function of the highest frequency of the system and the damping of the highest frequency mode. However, a simplified equation can be used to estimate the stability limit: $\triangle t_{st} = e/c_d$, where $e$ is the smallest mesh size used in the structure and $c_d = \sqrt{E/\rho}$ is the wave speed, in which $E$ is the modulus of elasticity and $\rho$ is the density. For the material used in this paper, $c_d$ = 5189 m/s (17024 ft/s). Hence, if the material does not change, the accuracy of the solution is governed by the mesh size. This paper utilizes the automatic time incrementation and stability option in ABAQUS [24]. This means that ABAQUS [24] determines the stability limit based on the mesh size and material properties and adjusts the time increment size during the analysis such that it does not exceed the stability limit.

The behavior of the system also depends on the load release time, $t_d$, as it simulates the sudden member loss and must be sufficiently small to ensure the load is rapidly released to zero. However, there is no clear guideline on how long $t_d$ needs to be. Therefore, before implementing the proposed procedure on the 3D FE model, a single beam is studied to determine the appropriate element type, mesh size, $e$, and load release time, $t_d$. This single beam case study also provides the comparison between *QSD* and *SD*.

### 5.1. Single beam study

This research uses a single beam case study to determine (1) element type, (2) mesh size, $e$, and (3) load release time, $t_d$, that will be used in the 3D FE model of the simply supported bridge, as well as a comparison of the *QSD* and *SD* methods.

The beam in this study has the same section size (W14×109) as the diagonal members in the simply supported bridge and a length of 3.05 m (10 ft) which is one half of the length of a diagonal member. The beam is fixed at one end - translational and rotational (if active) degrees of freedom are restrained in all three directions. The load is applied at the free end.

#### 5.1.1. Element type and analysis method

The effect of the element type on the dynamic response of the beam is first investigated. Three different elements types are considered: (1) C3DR8, 8-node reduced integration brick elements with three translational degrees of freedom per node, (2) S4R, 4-node reduced integration shell elements with three translational and three rotational degrees of freedom per node, and (3) B31, 2-node 3D linear beam with three translational and three rotational degrees of freedom per node [24]. For the brick and shell elements, enhanced hourglass control is used. For all three element types, the mesh size is 25.4 mm (1 in.).

The explicit dynamic analysis for each element type is performed using both *QSD* and *SD* methods. When the *QSD* method is used, the structure is initially unstressed. A tensile stress of 53.5 MPa (7.75 ksi) corresponding to the stress in D4 (indicated in Fig. 2) under Redundancy I load combination (to be discussed further in the next section), is applied at the edges of the top and bottom flanges and web at the free end of the beam utilizing the forcing function in Fig. 3A.

Prior to implementing the *QSD* method, modal analyses were conducted to determine the period of the first mode for each element type, from which the load rise time, $t_r$, and load hold time $t_h$ were calculated following the recommendation described earlier.

When the *SD* method is used, the initial (undamaged) state of the beam corresponds to that of D4 under the Redundancy I load combination. This initial state is imported into a dynamic analysis in which the 53.5 MPa (7.75 ksi) stress is applied in compression at the edges of the top and bottom flanges and web at the free end utilizing the forcing function in Fig. 3B. For both methods, the load release time, $t_d$, is 0.005 ms.

Regardless of element type or analysis method, the expected behavior is that after the load is released, a compressive wave travels along the beam at a rate of approximately the wave speed, $c_d$. This is demonstrated by tracing the axial stresses, acting at the center of gravity of the section, along the beam length. Fig. 4A shows the compressive stress wave that has propagated into the beam at time $t = 0.2$ ms after the load was released for all element types as well as analysis methods. It can be seen that all three element types along with both methods converge to approximately the same solution, with the wave having traveled about the same length of 1 m (3.3 ft), as expected.

As shown in Fig. 4A, the wave has similar path for the brick and shell elements but it is different for the frame elements, indicating that the frame elements are not capable of capturing the full dynamic behavior of the beam. There is a clear advantage of using shell elements due to their higher computational efficiency (as compared to brick elements). Therefore, this research utilizes shell elements for all bridge components in the 3D FE model. The study also verifies that both the *QSD* and *SD* methods provide the same response. The *SD* method is used in this paper due to the previously mentioned challenges in using the *QSD* method for the 3D FE model.

#### 5.1.2. Mesh refinement study

The mesh size is determined through a mesh refinement study, in which the beam is modeled with shell elements and the *SD* method is used. Four different mesh sizes, $e$, are considered: 6.35 mm (0.25 in.), 12.7 mm (0.5 in.), 25.4 mm (1 in.), and 50.8 mm (2 in.). The beam behavior is investigated by tracing the axial stresses, acting at the center of gravity of the section, along the beam length.

Fig. 4B shows the compressive stress propagating through the beam

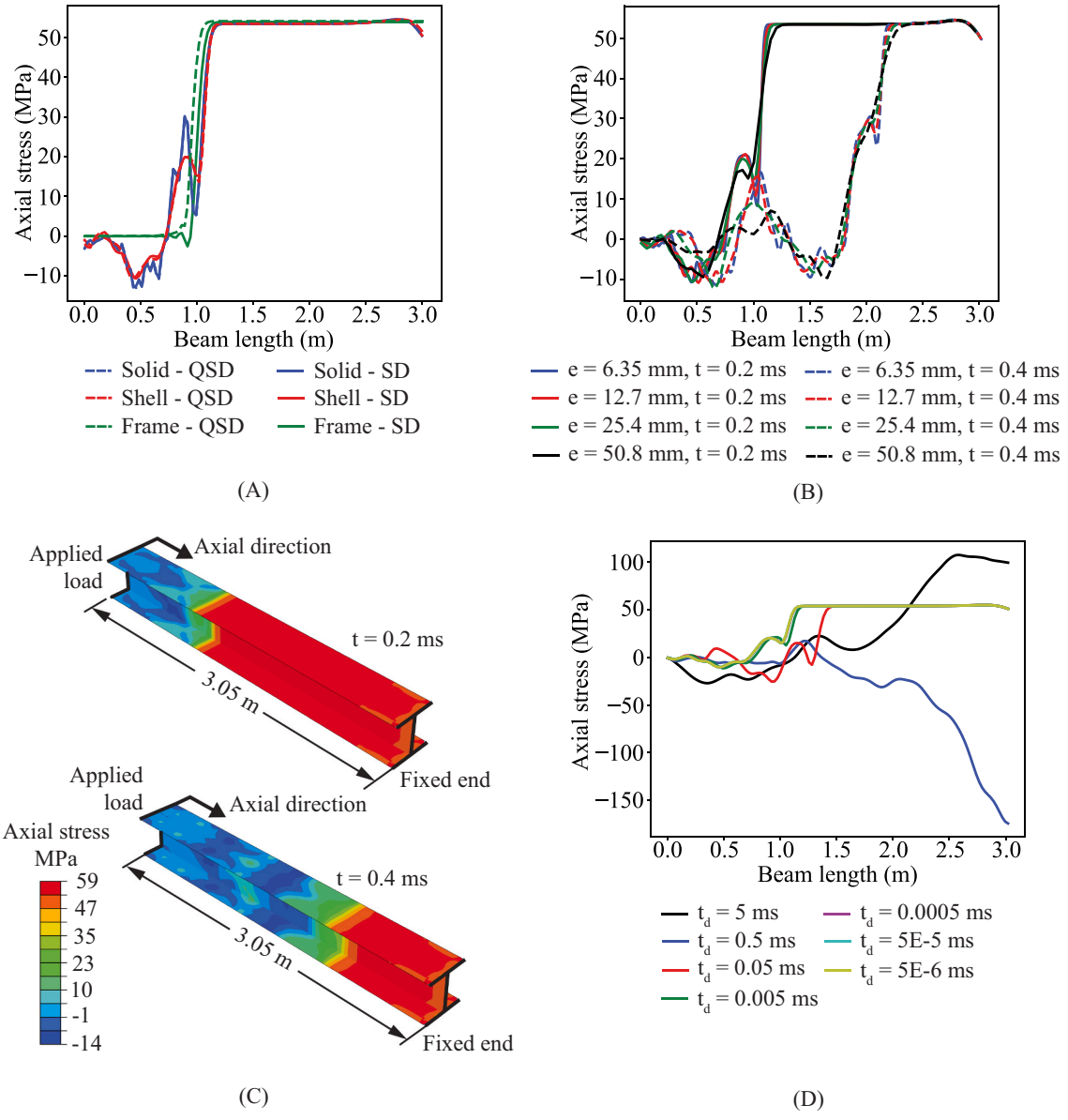


**Fig. 4.** Instantaneous dynamic behavior of single beam case study: (A) Element type and analysis method study, (B) Mesh refinement study, (C) Stress wave contour for a mesh size = 24.5 mm at two time instants, $t$ = 0.2 and 0.4 ms, and (D) Load release time, $t_d$, study.

at $t = 0.2$ and $t = 0.4$ ms after the load is released. The plot indicates that the beam response is similar regardless of the mesh size. Furthermore, for both times, the wave has traveled the expected 1 m (3.3 ft) and 2 m (6.7 ft), respectively, meaning that all mesh sizes result in a stability limit sufficiently small to achieve an accurate solution. The order of magnitude of the stability limit determined using the simplified equation given earlier in this paper is $10^{-6}$, which is also what ABAQUS [24] uses in the analysis. A slight difference in the wave path is noticeable for the beam with the 50.8 mm (2 in.) mesh size. Based on these results, the selected mesh size to be used in the 3D FE model is 25.4 mm (1 in.).

Fig. 4C presents the axial stress contour of the beam for the 25.4 mm (1 in.) mesh size which clearly shows the wave path for $t = 0.2$ and $t = 0.4$ ms. The initially stressed beam experiences load reduction as the wave propagates through, which is demonstrated by the change in color in the stress contour. For example, at time $t = 0.2$ ms, approximately two-thirds of the beam (measured from the fixed end) maintains its initial load, defined by the red stress contour in Fig. 4C. The slight oscillations that are seen in Fig. 4B can also be identified in the stress contour.

### 5.1.3. *Load release time*

To understand the effect of the load release time, $t_d$, a sensitivity study was conducted in which a range of times, $t_d$, between $5E-6$ ms and 5 ms were investigated. The beam was modeled with 25.4 mm (1 in.) mesh size shell elements and the *SD* method was used. The beam response is demonstrated by tracing the axial stresses, acting at the center of gravity of the section, along the beam length, at a time, $t = 0.2$ ms, after the load was released for each of the investigated times, $t_d$. This is shown in Fig. 4D.

It is evident that the time to release the load to zero has a significant effect on the behavior. As $t_d$ becomes longer, the wave starts propagating through the beam before the load is completely reduced to zero. For example, $t_d = 0.05$ ms results in a wave that travels approximately 1.5 m (4.9 ft) which is longer than the expected 1 m (3.3 ft). Because the wave speed and the time are constant in this case, the cause of this difference is that the wave is in the beam before the load reaches zero. The much higher stresses for $t_d$ above 0.05 ms indicate that the wave has already propagated through the beam, reflected at the fixed end, and traveled back towards the free end, and that likely happened several times. As

shown in Fig. 4D, release times below $t_d = 0.05$ ms converge to the same results, with the wave traveling approximately the same length of the expected 1 m (3.3 ft). Thus, the 3D FE model uses $t_d = 0.0005$ ms.

### 5.2. Simply supported vehicular bridge

The instantaneous loss of a diagonal member (D4) of the simply supported, two-lane vehicular bridge is investigated through an explicit dynamic analysis which utilizes the findings from the single beam study as follows: all bridge components are modeled with shell elements and 25.4 mm (1 in.) mesh size, the release load time is $t_d = 0.0005$ ms, and the *SD* method in which the dynamic analysis is performed on the initial (undamaged) deformed shape of the bridge is used. Note that damping was not included in the dynamic analysis. This is primarily because the high velocity stress wave propagates rapidly resulting in an instantaneous impact for which damping would not yet be activated. It is also conservative to ignore the effect of damping.

For the *SD* analysis method, the initial (undamaged) stress state as well as the tensile force in the failed diagonal member need to be known prior to performing the dynamic analysis. This initial stress state is found through a static analysis of the bridge in which the Redundancy I load combination developed in Connor et al. [14] and AASHTO Guide Specifications [15] is used:

$$\text{Redundancy I}: \ (1 + \text{DA}_R)(1.05\text{DC} + 0.85\text{LL}) \tag{1}$$

where *DC* is the dead load of the bridge components, *LL* is the vehicular live load, and $DA_R$ is the dynamic amplification factor. The dead load includes the self-weight of the structural steel components as well as a 1.25 kN/m$^2$ (25 psf) lightweight deck. The live load includes two lanes of vehicular traffic corresponding to 18.7 kN/m (1280 lbs/ft) uniformly distributed lane load and two design trucks positioned to produce the worst effect [8]. The dynamic amplification factor, $DA_R$ intended to be used in a static analysis to account for the inertia effects associated with member damage. Because in this paper an explicit dynamic analysis is performed, this dynamic amplification factor is not needed (i.e., $DA_R$=0).

Once the initial (undamaged) stress state is found, it is then imported into the explicit dynamic analysis in which diagonal member, D4 in Truss Plane 1, is severed by removing 50.8 mm (2 in.) from the geometry along its midsection. The tensile stress of 53.5 MPa (7.75 ksi) acting at that section is applied at the flange and web edges in compression very rapidly at time $t_d$ as shown in Fig. 3B. The dynamic analysis is continued for 1 ms. This short time duration allows for a large number of time increments (at every 0.0002 ms) to be recorded, providing a high-fidelity time history of the stress wave propagating through the diagonal member into the adjacent modular joints. Note that, in this case the entire cross section of the beam is severed which is considered conservative and simulates unstable crack propagation. Thus, if the beam had a larger cross section, the size of the fracture would increase, resulting in higher energy release and hence, a larger stress applied at the fractured surface. The compressive stress wave then propagates within the same time frame but with higher intensity, ultimately increasing the strain rates measured in the modular joint components.

Fig. 5A shows the axial stress contour at time, $t = 0.3$ ms, after fracture has occurred. At this time, the high-velocity stress wave traveled approximately half of the undamaged portion of D4, or around 1.52 m (5 ft). The axial stress time history is recorded at this location and is presented in Fig. 5B. The instant the high-velocity stress wave has reached the section is clearly indicated by the sudden change in stress from the initial (undamaged) magnitude of 53.5 MPa (7.75 ksi) to approximately zero.

To further investigate the high-velocity stress wave impact on the diagonal member, the strain rates at the section cut indicated in Fig. 5A are calculated. Note that right at the vicinity of the fracture, the strain rates are expected to be the highest, and at sections further from the fracture, the strain rates should decrease. The strain rate is measured as the change in strain between two time instants, where strain is calculated using the axial stress in the element and the modulus of elasticity. The region with the biggest change in the shortest time is considered (marked in Fig. 5B). As expected, high strain rates are measured in the diagonal member: 2.02, 2.09, and 3 /*s* for the top flange, bottom flange, and web respectively. These strain rates are much higher than the intermediate strain rates of $10^{-3}$/s which are typically associated with undamaged bridges under live load. As the diagonal members are hot rolled as opposed to built-up welded sections, the high strain rates are not expected to further compromise the section.

Because the stress wave travels at a very high rate [$c_d = 5189$ m/s (17024 ft/s)], it reaches the modular joints connecting the damaged diagonal member (LJ5 and UJ4, where LJ indicates lower chord joint, and UJ indicates upper chord joint) in just 0.59 ms. Once the wave propagates into the joint, it disperses in different directions along the web and the flanges, and also travels back into the severed diagonal

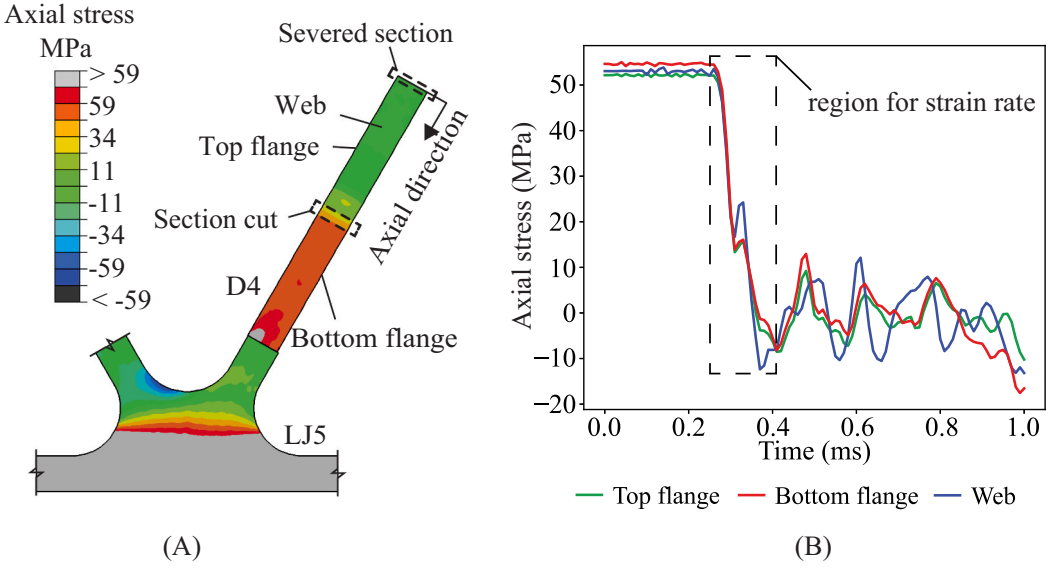


**Fig. 5.** Instantaneous dynamic behavior of the damaged diagonal: (A) Compressive stress wave contour at time $t = 0.3$ ms and (B) Axial stress time history for section cut.

member. The response of the modular joint to the impact of the compressive stress is investigated by recording the von Mises stress time history at several sections in the starter segments (Side R, Chord R, Side L, Chord L) and the bent flange plates (Bend R, Bend T, Bend L) of the lower chord modular joint LJ5 (sections indicated in Fig. 2). For the purpose of this investigation, the dynamic analysis is continued to 10 ms, which provides enough time for the wave to reach these sections. As the analysis time is longer, to save computational resources, the results are recorded at every 0.002 ms which still provides a high-fidelity time history of the stress wave propagating through the modular joint. The stress time histories are presented in Fig. 6 and Fig. 7. Additionally, the von Mises stress contours of the wave passing through the sections are shown in Fig. 8.

The instant the wave passes through the sections is distinctly defined by the sudden change in von Mises stress in the time history diagrams (Fig. 6). Side R, being closer to the severed diagonal member D4 has the highest von Mises stress change which is particularly noticeable in the middle flange. When the stress wave propagates through Side R, the von Mises stress in the middle flange decreases from the initial value of 86 MPa (12.5 ksi) to approximately 20 MPa (3 ksi). Similar behavior is seen in the right flange and the web. However, as the wave passes through Side R, the von Mises stress in the middle flange begin to increase with peak value of 101 MPa (15 ksi) which is likely due to the middle flange plate having smaller thickness than the right flange and web plates. Fig. 8 clearly shows that the initially stressed Side R experiences load reduction as the wave propagates through, which is demonstrated by the change in color in the stress contour. Side L has a similar behavior with the stresses in the middle flange being much higher than the stresses in the left flange and web. However, the change in von Mises stress is smaller (Fig. 6). The peak von Mises stress of 119 MPa (17 ksi) is recorded in the middle flange which is approximately 47 MPa (7 ksi) increase from the initial stress. The change in von Mises stress in Chord R and Chord L are very small as it can be seen in Fig. 6. This is also evident from Fig. 8, as the stress contour in these sections does not significantly

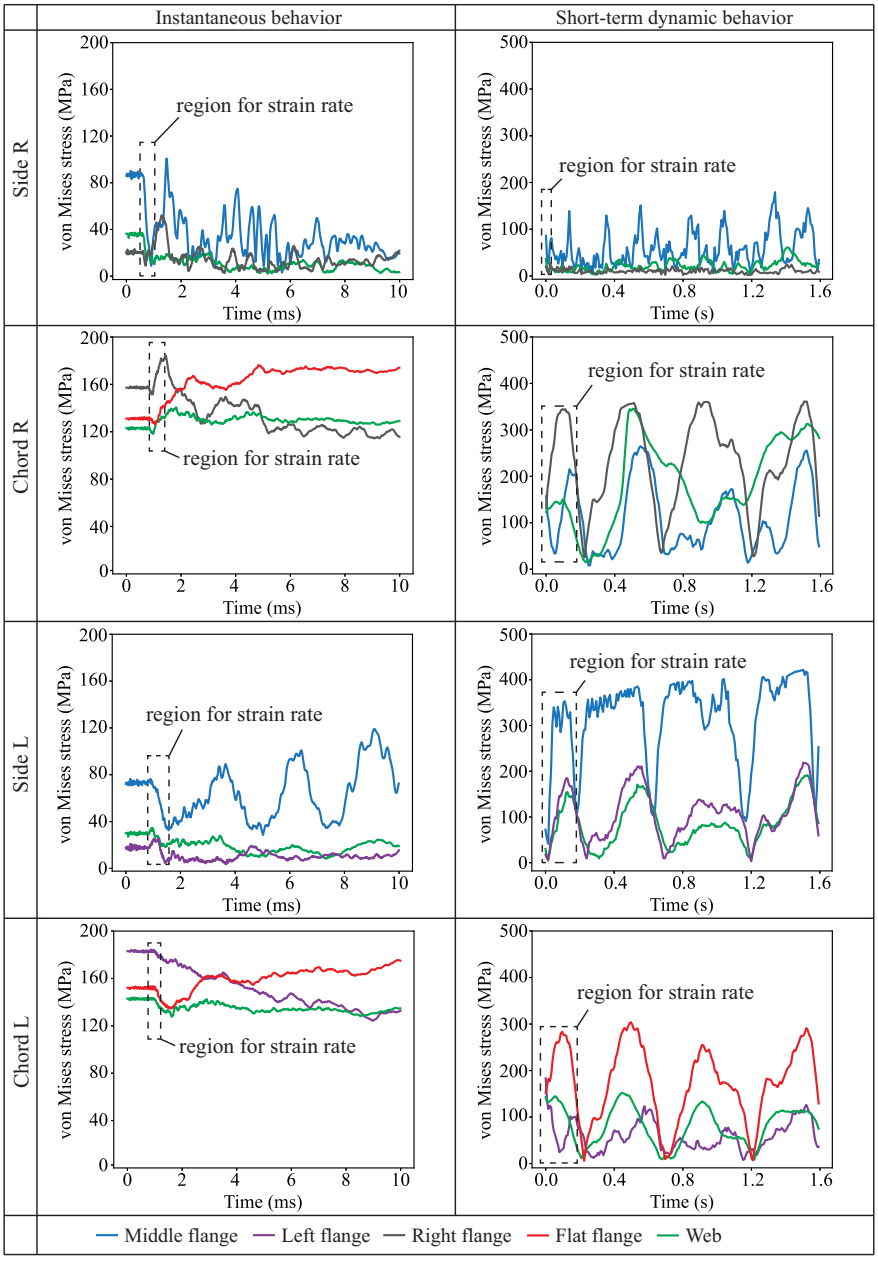


**Fig. 6.** Instantaneous and short-term dynamic behavior of lower chord modular joint LJ5: von Mises stress time history at the starter segments (see Fig. 2).

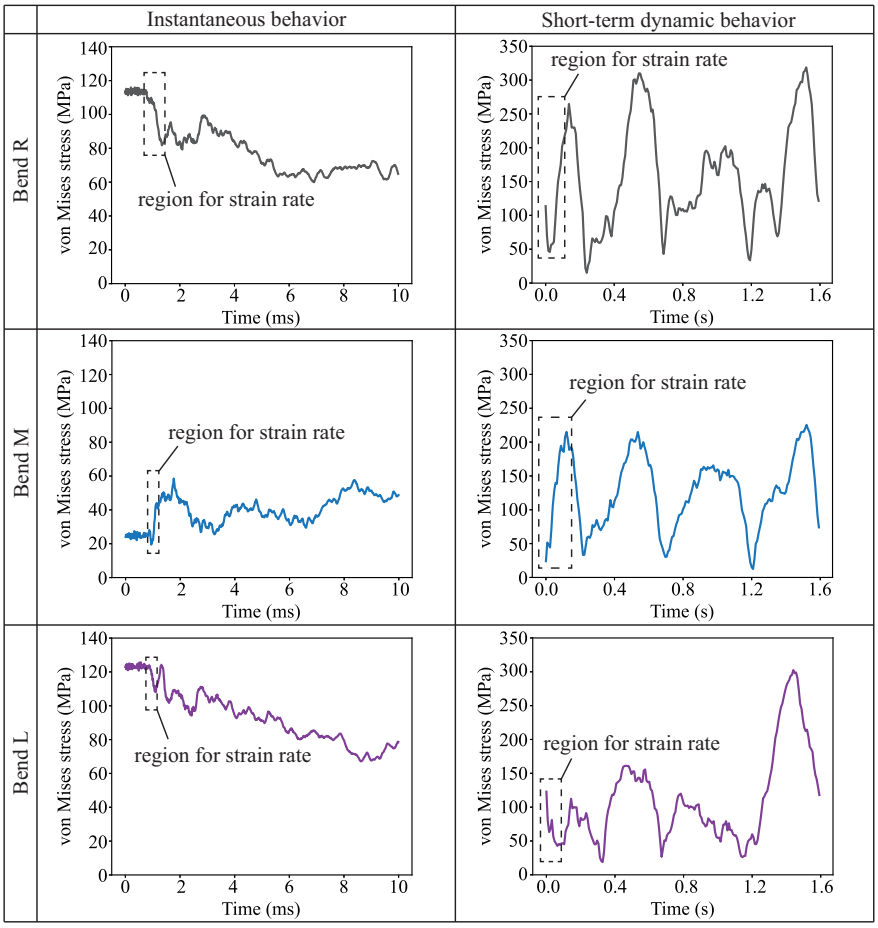


**Fig. 7.** Instantaneous and short-term dynamic behavior of lower chord modular joint LJ5: von Mises stress time history at the bent plates (see Fig. 2).

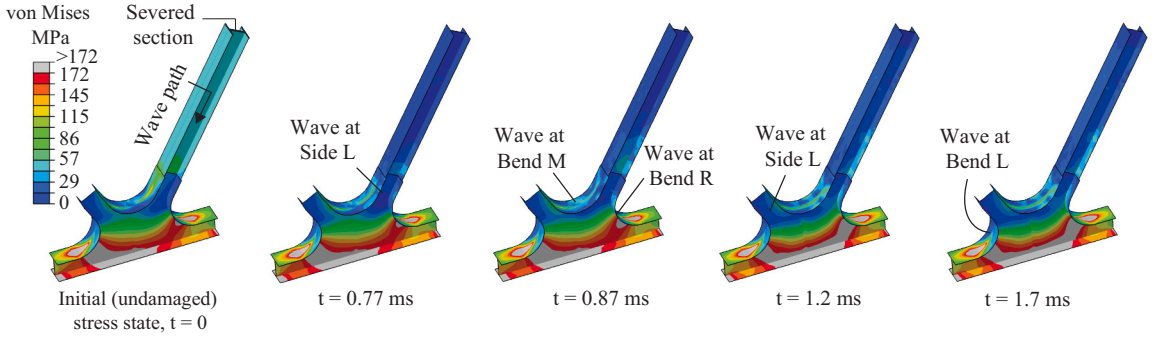


**Fig. 8.** Instantaneous dynamic behavior of lower chord modular joint LJ5: von Mises stress contours, as the stress wave is propagating through each of the sections.

change.

The behavior of the bent flange plates follows similar trend with Bend M and Bend R having higher von Mises stress change compared to Bend L (Fig. 7). This is expected behavior, as both sections are closer to the fractured diagonal and thus, the wave propagates with higher intensity. Bend R experiences an instantaneous reduction in von Mises stress from its initial value of 114 MPa (16 ksi) to approximately 82 MPa (11.9 ksi), which is relatively low. As shown in Fig. 7, the sudden change in von Mises stress in Bend M increases the initial stress [24 MPa (3.5 ksi)], indicating that this section is initially in compression and accumulates compressive stresses as the high-velocity stress wave passes through which is also observed by the change in the stress contour in Fig. 8. The von Mises stress in Bend M continues to increase in time with peak value of 58 MPa (8.5 ksi). Fig. 7 and Fig. 8 show that Bend L experiences a very small change in von Mises stress [around 15 MPa (2.15 ksi)]. This is expected, as this sections is further away from the fractured diagonal member. Overall, the sudden change in von Mises stress in the bent regions is found to be relatively small. This behavior can also be observed from Fig. 8, as the stress contour does not significantly change as the wave is passing through the bent plates.

The von Mises stress time histories in Fig. 7 as well as the stress contours in Fig. 8 indicate that none of the sections yield due to the instantaneous impact of the high-velocity stress wave. However, as the modular joint is composed of welded and cold bent flange plates, resulting in a reduced fracture toughness, there is a potential for further reduction in fracture toughness due to high strain rates (above $10^{-3}$/s).

Strain rates associated with abrupt member loss need to be considered in the design of the modular joint system, such that the modular joint is protected from fracture. While the system is able to tolerate the loss of a diagonal member, it would not be able to redistribute load if a modular joint is lost. Table 1 presents strain rates calculated for each section. As expected, the strain rates are the highest in Side R because of its proximity to the damaged diagonal member and lower strain rates are measured in the other sections. However, the strain rates measured in the bent flange plates are significantly higher than the intermediate strain rates of $10^{-3}$/s measured in undamaged bridges under live load. Thus, strain rates associated with sudden member loss need to be considered in design so that the modular joint is protected and fracture in any of the plates does not occur. Limiting the bend radius of the flange plates as a function of the plate thickness as well as using steel plates that exceed the minimum CVN requirements for the selected application increase the fracture toughness of the steel and thus, would be beneficial for the modular joint.

## 6. Short-term dynamic behavior

This section focuses on the short-term dynamic behavior of the bridge following the sudden loss of diagonal member, D4. The dynamic analysis from the previous section is continued to 2 s. Conservatively, damping was not used in this short-term dynamic analysis. In this section, the lower and upper chord members as well as the diagonal members (not indicated in Fig. 2) are labeled based on the modular joints they connect. For example, L4-5 indicates lower chord member connecting lower chord joints LJ4 and LJ5; D5-5 indicates a diagonal member connecting lower chord joint LJ5 and upper chord joint UJ5; U4-5 indicates an upper chord member connecting upper chord joints UJ4 and UJ5.

### 6.1. System behavior

As the modular joints are able to respond to the impact of the high-velocity stress wave and also redistribute the load into the adjacent members, this section investigates the short-term dynamic behavior of the entire system. This corresponds to the state of the structure after load has been released and the effect of the instantaneous impact has diminished and is recorded for a longer time period. The focus is on the ability of the members and the structure to continue carry load after member loss which is evaluated by recording the change in vertical displacements at midspan as well as the von Mises stress contour of the system response.

The change in vertical displacements through time is recorded at the midsection of the lower chord member located at midspan, for both truss planes (fractured diagonal member D4 is in Truss Plane 1) and is presented in Fig. 9. As the free vibration phase continues, at approximately $t = 1.6$ s, the stresses in the upper chord joint UJ5 were found to exceed the ultimate stress of 483 MPa (70 ksi) as shown in Fig. 10D. Therefore, the results are only given for the time frame between zero and 1.6 s.

The displacement in the initial (undamaged) state are also presented in Fig. 9. The peak initial (undamaged) displacements in both truss planes is -389 mm (-15.3 in). In the free vibration phase, after member loss, the displacements in both truss planes oscillate approximately with the same magnitude that is close to the initial, indicating that the system maintains stability and continues to carry load. The peak positive displacement of 454 mm (17.9 in.) is recorded at time $t = 0.496$ s in Truss Plane 1 while the peak negative displacement of -375 mm (14.8 in.) is recorded at time $t = 0.952$ s in Truss Plane 2. The difference in response between the two truss planes is expected with larger displacements recorded in Truss Plane 1. This is because the fracture is only in Truss Plane 1 and therefore, load is primarily distributed to its members, particularly in the beginning of the free vibration phase.

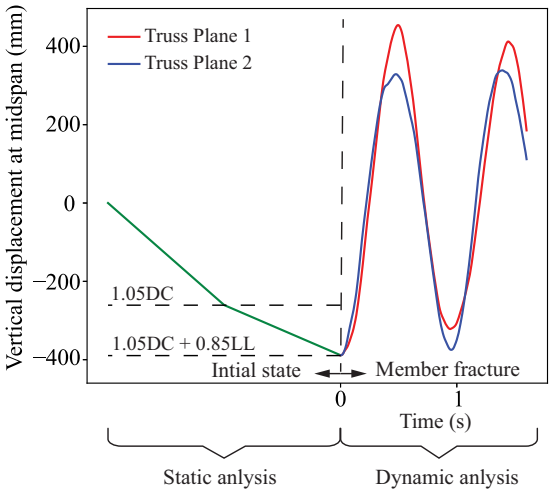


**Fig. 9.** Short-term dynamic behavior: vertical displacements at midspan lower chord member.

The magnitude of the displacement indicates that some sections in the chords are yielding during the free vibration phase. Fig. 10 presents the response of the system through the von Mises stress contour for different times after member is severed. Fig. 10A shows the initial (undamaged) stress state. Approximately at $t = 0.42$ s, the top flange of the lower chord member, L4-5 in Truss Plane 1, reaches the yield stress at the side with joint LJ4 (Fig. 10B). At the same time, $t = 0.42$ s, the top flange of the upper chord member, U4-5 in Truss Plane 1, at the side with joint UJ5 begins to yield as well (Fig. 10B). The opposite lower chord and upper chord members in Truss Plane 2, at $t = 0.42$ s maintain their initial stress state, indicating that Truss Plane 2 is not engaged yet. With time, more sections of members L4-5 and U4-5 in Truss Plane 1 begin to yield. As shown in Fig. 10C, at time $t = 0.56$ s, larger potion of the top flange of member U4-5 at the side with joint UJ5 has reached yield stress. Similar behavior is observed but in the bottom flange of U4-5 at the side with joint UJ4. The von Mises stress contour presented in Fig. 10D shows that, as the system continues to vibrate, the stresses in the chords in both truss planes have increased with some sections reaching above the yield stress, clearly demonstrating the redistribution of the load along the bridge span.

The stress contour in Fig. 10D also indicates the 3D beahavior of the system regardless of having only one truss plane compromised. In addition, the deformed shape shows that the members in Truss Plane 1 closer to the fractured diagonal member experiece out-of-plane movement, further demonstrating the 3D behavior.

As shown in Fig. 10E, at time $t = 1.6$ s, the middle bent flange of the upper chord joint UJ5 is stressed up to the material's ultimate stress of 483 MPa (70 ksi). This is likely due to the increased stress in the diagonal member D5-5. In its initial state, member D5-5 has very small, close to zero compressive stresses. However, due to the fractured diagonal D4, the stresses in sections Side R and Side L of joint LJ5 increase significantly (Fig. 6), which are then transferred through the diagonal member

**Table 1**
Strain rate associated with instantaneous dynamic behavior of modular joint LJ5 (sections indicated in Fig. 2).

| | Strain rate (/s) | | | | | | |
|---|---|---|---|---|---|---|---|
| | Side R | Chord R | Side L | Chord L | Bend R | Bend M | Bend L |
| Middle flange | 1.82 | NA | 0.252 | NA | NA | 0.663 | NA |
| Right flange | 1.02 | 0.334 | NA | NA | 0.583 | NA | NA |
| Left flange | NA | NA | 0.126 | 0.24 | Na | NA | 0.208 |
| Flat flange | NA | 0.171 | NA | 0.158 | NA | NA | NA |
| Web | 0.61 | 0.174 | 0.488 | 0.122 | NA | NA | NA |

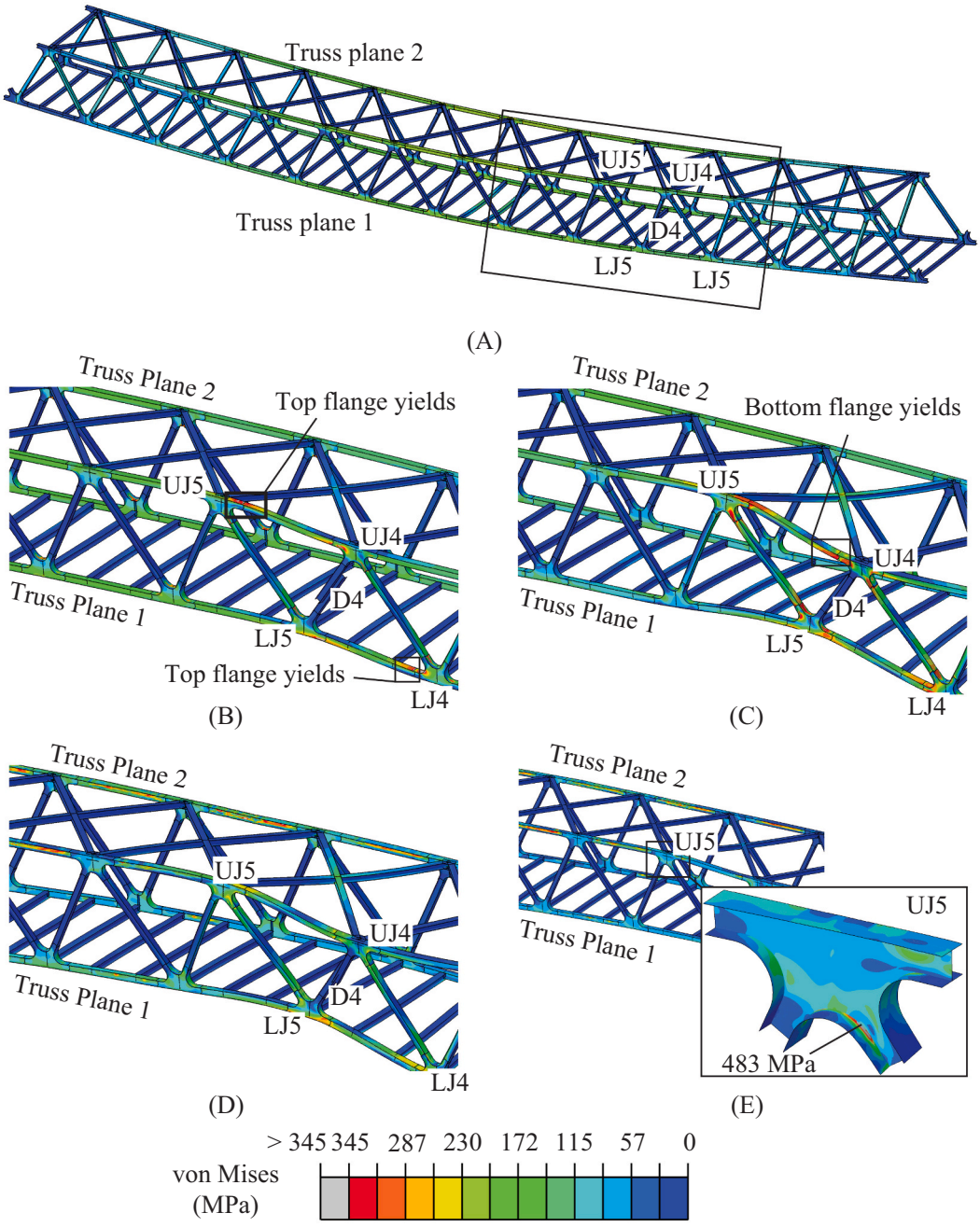


**Fig. 10.** Short-term dynamic behavior through von Mises stress contours of the system at: (A) Initial (undamaged) state, (B) Time $t = 0.42$ s, (C) Time $t = 0.56$ s, (D) Time $t = 1.56$ s, and (E) Time $t = 1.6$ s.

D5-5 to joint UJ5. This can be seen in Fig. 10B and Fig. 10C. In addition, the starter segment of joint UJ5 is also initially in compression, and the failed elements are exactly at the bend region of the middle flange plate which has relatively small thickness of 12.7 mm (0.5 in.), further contributing to the high stresses in the upper chord joint. After $t = 1.6$ s, the stresses in the system start to increase and the structure likely becomes unstable. However, the results clearly show that the modular joints are capable of redirecting load to the members adjacent to the fractured diagonal member and these members are able to sustain that additional load. Furthermore, as the system continues to vibrate, Truss Plane 2 significantly contributes in carrying the load thereby providing additional capacity.

Overall, the short-term dynamic analysis demonstrated the ability of the modular joint system to continue to carry load through flexure after a diagonal member is damaged.

### 6.2. *Local behavior: lower chord modular joint LJ5*

The short-term dynamic behavior of the lower chord modular joint LJ5 is investigated by recording the von Mises stress time history at the four sections in the starter segments and the three sections in the bent region of the flange plates, shown in Fig. 6 and Fig. 7 respectively. The peak von Mises stresses at each section are presented in Table 2.

As the system is let to vibrate freely, the von Mises stress in the middle flange of section Side R continues to increase with peak value of 184 MPa (27 ksi). The out-of-plane movement of the fractured diagonal

**Table 2**
Peak von Mises stress associated with short-term dynamic behavior of modular joint LJ5 (sections indicated in Fig. 2). NA = not available

| | von Mises stress (*MPa*) | | | | | | |
|---|---|---|---|---|---|---|---|
| | Side R | Chord R | Side L | Chord L | Bend R | Bend M | Bend L |
| Middle flange | 184 | NA | 447 | NA | NA | 225 | NA |
| Right flange | 30 | 265 | NA | NA | 319 | NA | NA |
| Left flange | NA | NA | 219 | 183 | NA | NA | 302 |
| Flat flange | NA | 365 | NA | 304 | NA | NA | NA |
| Web | 61 | 346 | 191 | 151 | NA | NA | NA |

D4, in combination with the relatively small thickness of 12.7 mm (0.5 in.) of the middle flange plate are likely the cause of the high stresses. Section Side L experiences similar behavior. However, the recorded peak von Mises stress of 447 MPa (65 ksi) is much higher and close to the ultimate stress of 483 MPa (70 ksi). The von Mises stress in the left flange and web plates increases as well. This behavior indicates that the undamaged diagonal member, D5-5, significantly contributes to the redistribution of the load when D4 is damaged, which can also be seen in Fig. 10. The high stresses in the middle flange are also caused by the out-of-plane movement of the fractured member D4 and thinner middle flange plate. The middle flange plate has a thickness of 12.7 mm (0.5 in.) that was selected through the optimization approach in Tumbeva et al. [1]. However in Tumbeva et al. [1], under all load scenarios, the forces acting in the middle flange plate were found to be very small, close to zero. Increasing the thickness of the middle flange plate would potentially reduce the stresses in the bent region to provide higher safety when a diagonal member is damaged.

The stress contours in Fig. 10B and Fig. 10C as well as the time histories for sections Chord R and Chord L given in Fig. 6, indicate that the chord starter segments of LJ5 are able to respond to the sudden change in structure's geometry through flexure, thereby providing a path for the load to be redirected to the adjacent members. As section Chord R is right under the fractured member, stresses are expected to be higher than the stresses in section Chord L. The von Mises stresses in the web of section Chord R have reached the yield point, while the von Mises stresses in the flat flange are above the yield stress with peak value of 365 MPa (53 ksi). Lower von Mises stresses are recorded in the right flange of the section with peak value of 265 MPa (38 ksi). Section Chord L experiences similar behavior but with the highest peak von Mises stress of 304 MPa (44 ksi) found in the flat flange, indicating that the section has not yielded during the free vibration period. Note that the initial (undamaged) stress state in both sections, Chord R and Chord L, is primarily axial. However, the recorded dynamic behavior of having different stresses in the right/left and flat flanges, indicates that if D4 is damaged, the chord segments of joint LJ5 are able to redistribute the load to the adjacent lower chord members, L4-5 and L5-6, through flexure.

Fig. 7 shows that none of the sections in the bent regions have yielded which is desirable since the flange plates are cold bent and welded to the web. Section Bend R has a peak von Mises stress of 319 MPa (46 ksi) which is the highest compared to the other sections, as expected, but it is considerably close to the yield stress. The stresses in Bend M are the smallest with peak von Mises stress of 225 MPa (33 ksi). The time history for Bend L shows that the section maintains stresses close to the initial stress of 123 MPa (18 ksi) up to approximately $t = 1.2$ s and then the stresses increase significantly reaching a peak value of 302 MPa (44 ksi).

The periodic response of the joint components that is shown in Fig. 6 and Fig. 7 is expected as the system oscillates freely when load is being redistributed away from the fractured member (this behavior is also observed from Fig. 9). The model does not include damping and thus, the response does not decay in time.

It is also important to investigate the effect of the free vibration phase on the strain rate behavior of the modular joint. Table 3 presents strain rates calculated for each section. Similar to the instantaneous dynamic behavior, strain rates are the highest in Side R and lower strain rates are measured in the other sections. Although the stresses recorded in the short-term dynamic behavior are much higher (Fig. 6 and Fig. 7), the measured strain rates are smaller in comparison with the measured strain rates in the instantaneous dynamic behavior (Table 1) and also are more consistent with the strain rates of $10^{-3}$/s that are typically associated with undamaged bridges under live load. This is primarily because the change in stress occurs over a larger time frame in the short-term dynamic response. Therefore, it is important that the analysis is capable of capturing the instantaneous dynamic behavior of the modular joint such that the associated strain rates can be measured.

The results presented in this section clearly indicate that the modular joint is capable of redistributing the load through the starter segments and bend regions of the flange plates. To potentially reduce the stresses in the flange plates, their thickness could be increased. The web thickness and/or depth could be increased as well, to accommodate the relatively high stresses developed in the bottom flange.

## 7. Static behavior of the faulted structure

The prior sections investigated the instantaneous and short-term dynamic behavior of the modular joint system following sudden loss of diagonal member D4. This section, instead, focuses on the long-term behavior of the faulted system under normal use, thus investigating a circumstance in which the damage has not been detected and vehicular traffic continues. To simulate such scenario, a diagonal member is individually removed from the geometry at the beginning of the analysis. This study considers diagonal members D1 through D6 (Fig. 2) located in Truss Plane 1. The Redundancy II load combination developed in Connor et al. [14] and AASHTO Guide Specifications [15] which is similar to the Strength I load combination in American bridge design code [8] is used:

$$\text{Redundancy II}: \ 1.05\text{DC} + 1.30(\text{LL} + \text{IM}) \tag{2}$$

where *IM* is the dynamic live load allowance factor (*IM* = 15%). The dead load, *DC*, and the live load, *LL*, are the same as in the previous section.

The 3D FE model shown in Fig. 2 and detailed earlier is used to perform an implicit nonlinear static analysis in which a single diagonal member is removed. Dynamic effects associated with sudden member loss are ignored (i.e., the diagonal member was simply not included in the model from the start).

Fig. 11A compares the load-displacement behavior of an undamaged structure to the structure with different diagonal members removed (i.e., each damaged structure has one diagonal member removed, with the removed member identified in the legend). Displacements are measured at the midsection of the lower chord member located at midspan in Truss Plane 1. For all damaged cases, except for D1, the structure is able to carry the full dead and live load, including load factors. It is not unexpected that the loss of D1 cannot be tolerated, as this is a region of high shear demand and thus, the forces in D1 are the highest. Note that the portal diagonal member is not part of this study. Although, the structure

**Table 3**
Strain rate associated with short-term dynamic behavior of modular joint LJ5 (sections indicated in Fig. 2). NA = not available.

| | Strain rate (/s) | | | | | | |
|---|---|---|---|---|---|---|---|
| | Side R | Chord R | Side L | Chord L | Bend R | Bend M | Bend L |
| Middle flange | $4.9E-2$ | NA | $1.1E-2$ | NA | NA | $7E-3$ | NA |
| Right flange | $1E-2$ | $6E-3$ | NA | NA | $7.7E-3$ | NA | NA |
| Left flange | NA | NA | $8.1E-3$ | $6.3E-3$ | NA | NA | $3.9E-3$ |
| Flat flange | NA | $7.8E-3$ | NA | $6.8E-3$ | NA | NA | NA |
| Web | $1E-2$ | $4E-3$ | $7.4E-3$ | $3.3E-3$ | NA | NA | NA |

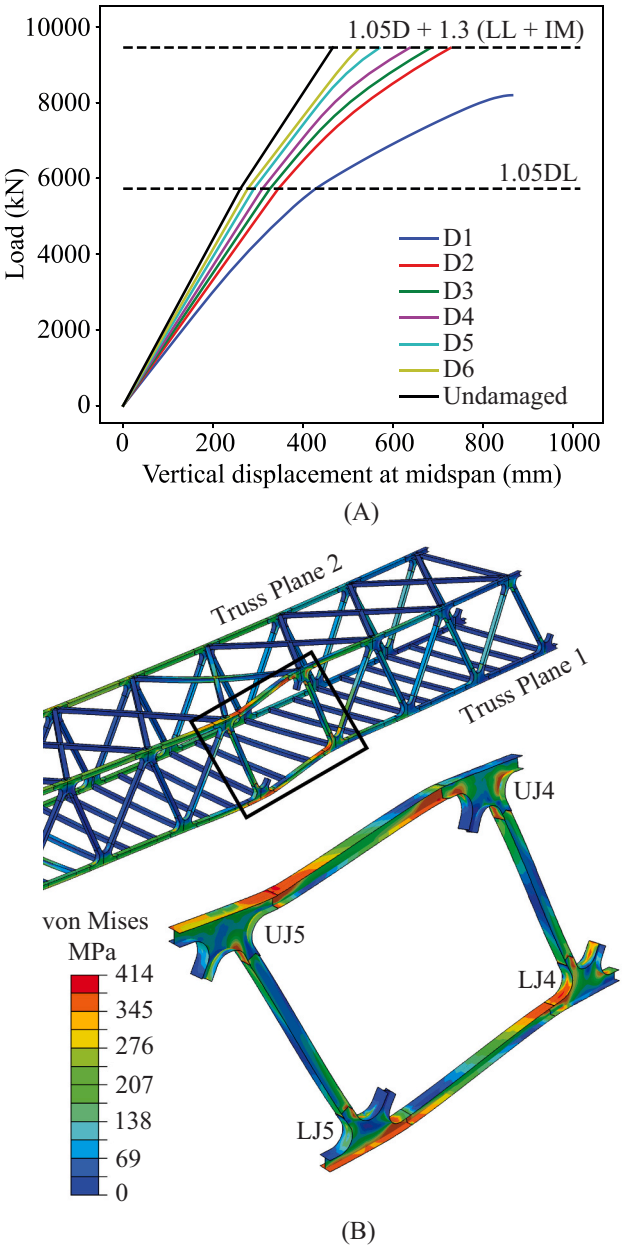


**Fig. 11.** Static behavior of the faulted structure: (A) Load-displacement curves for loss of diagonal members (numbers indicated in Fig. 2) and (B) von Mises stress contour for loss of D4.

is able to carry the full load in all cases except in D1, it is evident that the stiffness is reduced significantly, depending on which diagonal member is removed. The stiffness at the end of the load-displacement curve after the full load has been applied is compared to the initial elastic stiffness of the undamaged bridge. The initial elastic stiffness is determined by calculating the slopes between every two successive increments within the linear elastic region in the load-displacement curve, and taking their average. The end of the initial elastic region is defined at the point where two successive slopes differ more than 0.1%. Comparing all member loss cases (except D1), the D6 case is the most stiff, as it is able to maintain approximately 62% of its initial elastic stiffness, whereas the D2 case is the least stiff as it maintains just 40% of its initial elastic stiffness. This directly correlates with the shear demand (and the force in the diagonal), being less in the center of the span compared to the end. To mitigate the loss in stiffness, the chords and modular joints could be proportioned with greater depth.

Fig. 11B shows the von Mises stress distribution of the faulted structure when member D4 is removed. Similar to the short-term dynamic response, the members adjacent to the fractured member are affected the most. As expected, the stresses in the starter segments of the two modular joints connecting the removed D4 (LJ5 and UJ4) are zero. Overall, in the four modular joints (LJ4, LJ5, UJ4, and UJ5), the sections closer to D4 experience the highest stress concentration. This is especially noticeable in the flat flange of the lower chord joint LJ5 which has developed stresses above the yield stress [peak stress of approximately 413 MPa (60 ksi)], causing a significant decrease in the stiffness (Fig. 11A). However, none of the elements in the modular joints have developed stresses close to the ultimate stress of 483 MPa (70 ksi) thus, allowing the structure to remain stable. The stress contour in Fig. 11B indicates that the load that would have been in D4 is being redistributed through flexure to the surrounding members.

Fig. 11B clearly shows that the diagonal members closer to D4 are being significantly stressed, as a direct result of the fracture and load being redirected to the adjacent members. However, in typical design, without considering a member loss event, the diagonal members are designed for much smaller stresses, usually close to zero. Therefore, in the case of a sudden loss of a diagonal member, for the structure to continue carry load, the diagonal members adjacent to the fractured should be designed to sustain the transferred load. Furthermore, buckling of the compressive diagonal members should be considered such that the system is protected from losing another member. Fig. 11B also shows that the lateral bracing adjacent to the removed member as well as the opposite upper chord are engaged.

Overall, the global system behavior of the faulted structure was evaluated through a nonlinear static approach. The results demonstrated the ability of the modular joints to sustain the sudden loss of a diagonal member and redistribute the load through flexure.

## 8. Conclusions

This paper presented a numerical investigation of the redundancy of steel truss bridges composed of modular joints when subjected to sudden loss of diagonal member including the response of the system through nonlinear dynamic analysis and nonlinear static analysis.

This section includes recommendations for performing the dynamic analysis as well as summarizes major research findings.

### 8.1. Recommendations for numerical analysis

An explicit dynamic analysis was used to investigate the behavior of the modular joint system when subjected to sudden loss of a diagonal member. The results show that the analysis is able to capture the instantaneous response of the modular joints to the high-velocity stress wave as well as the short-term dynamic behavior of the system. It is particularly important that the strain rates developed in the cold bent and welded flange plates of the modular joint as a result of the high-velocity stress wave can be calculated from the analysis, as they are significantly above the intermediate strain rates typical of live load passage over a bridge and reduce the fracture toughness of the plates. This dynamic analysis would be most important in systems composed of welded components and/or bent plates.

The following recommendations on performing the dynamic analysis are suggested:

- The FE model should be developed using brick or shell elements which better capture the behavior of the structure under the high-velocity stress wave when compared to frame elements. Shell elements are more suitable in large-scale models due to their higher computation efficiency.
- A full 3D FE model that closely represents the structural system should be used due to the unsymmetrical behavior of a system when subjected to member loss. Modeling half or quarter of the system would reduce the computational expense, but would not be able to accurately capture the 3D load distribution that occurs.
- The mesh size of the shell elements should be selected such that the stability limit required in the explicit time integration rule is sufficiently small for the method to achieve an accurate solution. A mesh refinement study should be performed to establish appropriate mesh size. The simplified approach of calculating the stability limit could be used to approximate mesh size to start the mesh refinement study.
- The FE model should incorporate nonlinear material properties including strain hardening, as the structure is expected to redistribute load through ductile behavior and develop a collapse-resistant mechanism. In addition, as the system undergoes sudden changes in geometry causing the development of large deflections, nonlinear geometry should also be considered.
- The *SD* analysis method is more appropriate for evaluating structures with longer natural periods (e.g., above 1 s). This method requires a static analysis of the undamaged structure to establish an initial stress state. This initial stress state needs to be imported into a different model, therefore, the FE software should have this capability. The *QSD* analysis model could be implemented for short period structures (e.g., less than 1 s).
- For both the *SD* and *QSD* analysis methods, the load release time, $t_d$, must be sufficiently small to ensure that the load is applied instantaneously. A sensitivity analysis should be performed to establish load release time in which the stability limit could be used as a starting point. Expected load release times are in the order of 0.0005 ms.

The proposed dynamic approach, for evaluating both instantaneous and short-term dynamic behavior, is suitable for other steel structures with other forms (i.e., variable-depth), different span arrangements (e.g., three-span continuous system), and span lengths as well as systems that are not composed of modular joints.

### 8.2. Summary of behavior

This paper presented a numerical investigation of the redundancy of the modular joint system for the case of a 119-m (390-ft) simply supported, two-lane [9.91-m (32.5-ft) wide] vehicular bridge, focusing on three behaviors: (1) instantaneous dynamic behavior, focusing on the effect of the high-velocity stress wave, with its associated high strain rates and impact on fracture toughness particularly in the cold bent and welded portion of the modular joint, (2) short-term dynamic behavior of the structure, and (3) static behavior of the faulted structure. Major findings and conclusions specifically relevant to this structural system include:

- Dynamic and static analyses demonstrated that the modular joint is able to redistribute load through flexure when a diagonal member is lost.
- High-velocity stress waves should be considered to evaluate minimum fracture toughness requirements. As a result of the instantaneous impact of the stress wave on the modular joint, strain rates in the cold bent and welded flange plates were found to be significantly higher than the intermediate strain rates of $10^{-3}$/s that are typically associated with undamaged bridges under live load. These higher strain rates (associated with member loss) lower the fracture toughness of the flange plates, which in combination with the reduced fracture toughness of the flange plates due to cold bending and welding, require a particular consideration in design for sudden member loss, such that the modular joint is protected and fracture in any of the cold bent plates does not occur.
- Current AASHTO provisions prescribe minimum toughness of steel using CVN requirements based on thickness and service temperature. However, it should be noted, that the minimum CVN requirements are in terms of the as-rolled condition of the plate and does not directly account for the change in fracture toughness due to welding and forming of the steel. Additional requirements associated with welding and cold bending of the plates must also be met to ensure enough toughness. It is therefore, recommended that fabrication of the modular joints is according to the Fracture Control Plan specified in the AASHTO/AWS (American Welding Society) D1.5M/D1.5 Bridge Welding Code [27]. In addition, especially when considering dynamic strain rates, having plates that exceed the minimum CVN requirements is beneficial. A sensitivity analysis to account for toughness based on various factors (temperature, thickness, bend radius, etc.) would be an important area for future research.
- Modular joints should be capacity-protected, such that yielding is forced into the members framing into it. This allows the modular joints to continue to redistribute load and prevent system collapse. The web and flanges bolted splice connections should be capable of developing the capacity of the diagonal or chord.
- As the structure was let to oscillate freely in the short-term dynamic analysis, stresses close to the ultimate stress of the material were found in the upper chord modular joint adjacent to the fractured diagonal, shortly after the load was released. Increasing the thickness of the middle flange plate would potentially reduce the stresses and provide higher safety of the system in case a diagonal member is damaged. Thicker web plate could also be beneficial.
- Both, static and dynamic analyses indicated that the diagonal members adjacent to the fractured member experience increased stress as a result of the load redistribution. This can cause buckling in the compressive diagonal members and needs to be considered in design to ensure that failure of these members does not occur and the system is protected from becoming unstable.
- The nonlinear static analysis indicated that the system is able to carry the full, factored dead and live load (Redundancy II load case, analogous to Strength I limit state), albeit at a reduced stiffness, when any one of the diagonal members D2 through D6 is lost. The stiffness reduction can be mitigated by increasing the depth of the chords. The ability to proportion chord depth to tolerate diagonal loss is a distinct advantage of this modular system.
- A dynamic analysis is recommended to establish the load-path redundancy of the system. A static analysis is not able to capture the behavior of the entire system and misses important localized behavior.

- A dynamic analysis that is able to capture the instantaneous response of the modular joint and allows strain rates due to the high-velocity stress wave to be calculated, is recommended.

Overall, the modular joint system takes advantage of the aspects of steel trusses that have made them the dominant long-span bridge form over the last century (i.e., high efficiency, ease of design, and longevity) and overcomes barriers to truss use today: lack of redundancy and problematic gusset plates. Importantly, this research demonstrate that in the design of structures, member loss should be taken into consideration.

## Declaration of Competing Interest

The authors declare that they have no known competing financial interests or personal relationships that could have appeared to influence the work reported in this paper.

## Acknowledgments

This material is based upon work supported by the National Science Foundation under Grant No. CMMI-1351272 and Grant No. IIP-2044340. Mirela D. Tumbeva is also supported by the O.H. Ammann Research Fellowship. Support from these sources and the program managers is gratefully acknowledged.

## References

[1] M.D. Tumbeva, A.P. Thrall, T.P. Zoli, Modular joint for the accelerated fabrication and erection of steel bridges, J. Br. Eng. 26 (6) (2021) 04021022.
[2] FHWA, Steel Bridge Design Handbook: Redundancy, Federal Highway Administration (FHWA), Washington D.C, 2015.
[3] E. Covington, C. Engel, K. Kelly-Sneed, J. Noh, T.P. Zoli, Portsmouth memorial bridge replacement: an exploration of truss design without gusset plates, in: Proceedings of the 2013 SEI Illinois Chapter Lecture Series, 2013.
[4] J.G. Chen, T.M. Adams, H. Sun, E.S. Bell, O. Buyukozturk, Camera-based vibration measurement of the world war I memorial bridge in Portsmouth, New Hampshire, J. Struct. Eng. 144 (11) (2018) 04018207.
[5] V. Shahsavari, M. Mashayekhi, M. Mehrkash, E. Santini-Bell, Diagnostic testing of a vertical lift truss bridge for model verification and decision-making support, Front. Built Environ. 5 (92) (2019) 1–19.
[6] E.S. Bell, R.A. Medina. Evaluation of Gusset-less Truss Connection to Aid Bridge Inspection and Condition Assessment, Report No. FHWA-NH-RD-26962M, Federal Highway Administration (FHWA), Washington, DC, 2019.
[7] M. Mashayekhi, E. Santini-Bell, Fatigue assessment of the gusset-less connection using field data and numerical model, Br. Struct. 15 (1-2) (2019) 75–86.
[8] AASHTO, in: Load and Resistance Factor Design (LRFD) Bridge Design Specifications Customary U.S. Units, 9th Edition, American Association of State Highway and Transportation Officials (AASHTO), Washington, D.C., 2020.
[9] J. Barsom, Development of AASHTO fracture toughness requirements for bridge steels, Eng. Fract. Mech. 7 (3) (1975).
[10] R. Connor, J. Lloyd, Maintenance Actions to Address Fatigue Cracking in Steel Bridge Structures: Proposed guidelines and Commentary., NCHRP Project 20-07, Task 387, Purdue University, West Lafayette, IN, 2017.
[11] S.M. Marjanishvili, Progressive analysis procedure for progressive collapse, J. Perform. Construct. Facil. 18 (2) (2004) 79–85.
[12] M. Ghosn, F. Moses, Redundancy in Highway Bridge Superstructures., NCHRP Report No. 406, Transportation Research Board, National Research Council, Washington, D.C., 1998.
[13] M. Ghosn, J. Yang, D. Beal, B. Sivakumar, Bridge System Safety And Redundancy, NCHRP Report No. 776, Transportation Research Board, National Academies of Sciences, Engineering, and Medicine, Washington, D.C., 2014.
[14] R. Connor, J. Francisco, M. Bonachera, V. Amit, L. Zhichao, K. Cem, Fracture-critical System Analysis For Steel Bridges, NCHRP Report No. 883, Transportation Research Board, National Academies of Sciences, Engineering, and Medicine, Washington, D.C., 2018.
[15] AASHTO, in: Guide Specifications for Analysis and Identification of Fracture Critical Members and System Redundant Members, 1st Edition, American Association of State Highway and Transportation Officials (AASHTO), Washington, D.C., 2018.
[16] URS Corporation, Fatigue Evaluation and Redundancy Analysis., Bridge No. 9340, I-35W Over Mississippi River, Draft Report Prepared for Mn/DOT, Minneapolis, MN, 2006.
[17] H. Cha, L. Lyrenmann, R.J. Connor, A. Varma, Experimental and numerical evaluation of the postfracture redundancy of a simple span truss bridge, J. Br. Eng. 19 (11) (2014) 0401448.
[18] S. Yan, X. Zhao, Y. Lu, Collapse-resisting mechanisms of planar trusses following sudden member loss, J. Struct. Eng. 143 (9) (2017) 04017114.
[19] H.T. Khuyen, I. Eiji, Linear redundancy analysis method considering plastic region for steel truss bridges, J. Br. Eng. 22 (3) (2017) 05016011.
[20] Y. Goto, N. Kawanishi, I. Honda, Dynamic stress amplification caused by sudden failure of tension members in steel truss bridges, J. Struct. Eng. 137 (8) (2011) 850–861.
[21] S. Liu, F.M. Bartlett, W. Zhou, Alternative load paths in steel through-truss bridges: case study, J. Br. Eng. 18 (9) (2013) 920–928.
[22] T. Huu-Tai, K. Seung-Eock, Nonlinear inelastic time-history analysis of truss structures, J. Construct. Steel Res. 67 (12) (2011) 1966–1972.
[23] K. Miyachi, S. Nakamura, A. Manda, Progressive collapse analysis of steel truss bridges and evaluation of ductility, J. Construct. Steel Res. 78 (2012) 192–200.
[24] ABAQUS, ABAQUS/Standard Analysis User's Manual Version 6.14, Dassault Systemes, Waltham,MA, 2016.
[25] T.P. Zoli, R. Woodward, Design of long span bridges for cable loss, in: Proceedings of the 2005 IABSE Symposium: Structures and Extreme Events, Lisbon, 2005, pp. 17–25.
[26] R.B. Malla, P. Agarwal, R. Ahmad, Dynamic analysis methodology for progressive failure of truss structures considering inelastic postbuckling cyclic member behavior, Eng. Struct. 33 (5) (2011) 1503–1513.
[27] AASHTO/American Welding Society (AWS), D1.5M/D1.5:2020 Bridge Welding Code, American Association of State Highway and Transportation Officials (AASHTO), Washington, D.C., 2020.